Talanta 81 (2010) 187–196

Contents lists available at ScienceDirect

Talanta

journal homepage: www.elsevier.com/locate/talanta

Enantioselective recognition of D- and L-tryptophan by imprinted polymer-carbon composite fiber sensor

Bhim Bali Prasad*, Rashmi Madhuri, Mahavir Prasad Tiwari, Piyush Sindhu Sharma

Analytical Division, Department of Chemistry, Faculty of Science, Banaras Hindu University, Varanasi 221005, India

ARTICLE INFO

Article history:
Received 5 October 2009
Received in revised form
23 November 2009
Accepted 24 November 2009
Available online 29 November 2009

Keywords:
Enantioselectivity
Molecularly imprinted polymer-carbon composite
Fiber sensor
Differential pulse anodic stripping voltammetry
L- and D-Tryptophan

ABSTRACT

Electrochemical sensors demonstrating enantioselectivity to tryptophan enantiomers, with high selectivity and sensitivity, were fabricated by the use of a monolithic fiber of molecularly imprinted polymer-carbon composite. The recognition mechanism and performance of these sensors were evaluated by differential pulse anodic stripping voltammetry. The sensor imprinted for L-tryptophan not only discriminated the target from its analogues and other amino acids but also responded specifically in racemic mixture in aqueous, biological, and pharmaceutical samples. The binding kinetics of L-tryptophan was also established with the help of anodic stripping cyclic voltammetry and chronocoulometry. The detection limit for L-tryptophan was as low as 0.24 ng mL^{-1} (signal/noise = 3) which is appropriate for biomarking diseases, caused by an acute tryptophan-depletion, in clinical setting.

1. Introduction

Biological activity of the majority of synthetic and natural compounds (medicines, pesticides, biologically active food supplements, etc.) depends on their enantiomeric composition. For instance, proteins incorporating L-amino acids have wide applications in the production of pharmaceuticals and foods, while D-amino acids do not participate in protein synthesis except generating toxicity during functioning of living organisms. Therefore, the development of a chiral selective analytical technique and quantification of one enantiomeric isomer in a racemic mixture is very important in the food and pharmaceutical industries as well as in vivo/vitro clinical analysis. In spite of the major development of enantioselective synthesis, methods for enantioselective analysis are quite a few in numbers. Although conventional chromatography [1] and capillary electrophoresis [2] are reportedly useful for the determination of enantiomer purity, these are not suited for high-throughput screening, and are time-consuming with the use of suitable chiral selectors. Last decade has witnessed some enantioselective sensing devices as inexpensive alternative to time-consuming separation methods [3–6]. In this context several kinds of chiral selectors viz., cyclodextrins (CDs), crown ethers, macrocyclic antibodies, serum albumin, quinine/quinidine derivatives, and calf thymus DNA (ct DNA) have been used for chiral separations [7]. However, molecularly imprinted polymers (MIPs) have obviously an advantage over these conventional chiral selectors in terms of the ease of preparation, scalability, low material cost, and flexibility. Despite the enormous development of MIP technology, MIP-based sensors especially in the area of electrochemical sensing are very scarce. Although conventional macroporous, methacrylate, acrylate, acrylamide, and vinyl-based MIPs have widely been explored for the selective separation, they are not used in the sensor development for the reason known to their electrical insulating characteristics. As an alternate, electrochemical sensors which could selectively recognize D- and L-forms were fabricated with the use of conducting polymers such as polypyrrole [8] and over-oxidized polypyrrole films [9,10]. These sensors were found to be capable of conducting electron directly from the binding sites to the electrode surface. In this work, we have fabricated an enantioselective monolithic fiber of MIP-carbon composite where the non-conducting MIP layer has turned to be conducting in the presence of carbon particles (dispersed as organized strip). Unlike the general MIP-composite electrode preparation protocol [11,12], we have resorted to a fresh approach for in situ synthesis of MIP-carbon composite fiber via activator generated by electron transfer for atom-transfer radical polymerization (AGET-ATRP) technique. It may be noted that AGET-ATRP is convenient than conventional ATRP, because of in situ generation

* Corresponding author. Tel.: +91 9451954449; fax: +91 542 22368127.
E-mail address: prof.bbpd@yahoo.com (B.B. Prasad).

0039-9140/$ – see front matter © 2009 Elsevier B.V. All rights reserved.
doi:10.1016/j.talanta.2009.11.055

of lower oxidation state of metal for catalysis [13]. Such living radical polymerization technique is reportedly known to be creating homogeneous binding sites (cavities) within the MIP network [14].

The proposed MIP-carbon composite electrode was examined for the enantioselective sensing of D- and L-tryptophan (Trp) in aqueous and real samples. L-Trp is an essential amino acid found in proteins, foods and pharmaceuticals and its unbalances/deficiency may cause several chronic diseases, namely, schizophrenia, hallucinations, delusions [15], and several other neural and stress related diseases [16]. Literature survey revealed that enantioselective Trp analyses have been accomplished with chiral selectors (ct DNA, CDs) [7,17] and MIPs [18–20]. However, in these measurements selectivity and sensitivity were not satisfactory and none of the used technique could analyze L-Trp at trace-level that could be taken as effective biomarker particularly with stress related diseases (depression and physchosis) in hospitalized patients.

2. Experimental

2.1. Reagents

Acryloyl chloride (AC), carbon powder (1–2 μm), and p-nitrophenol (NP) were purchased from Loba Chemie (Mumbai, India). All solvents, dimethylsulphoxide (DMSO), acetonitrile (ACN), triethylamine (TEA), acetic acid (HOAc), chloroform, ethanol, and acetone were purchased from Spectrochem Pvt. Ltd. (Mumbai, India). Cupric chloride ($CuCl_2$) and 2,2′-bipyridyl (bpy) were purchased from BDH chemicals (England). Ethylene glycol dimethylacrylate (EGDMA), D- and L-Trp, and its interferents were provided by Fluka (Steinheim, Germany). All the chemicals were AR grade and used as received. Phosphate buffer solution (PBS), pH 2.0 (ionic strength 0.1 M), was used as a supporting electrolyte. Standard stock solution of Trp (1.0 μg mL^{-1}) was prepared using deionized triple-distilled water (conducting range 0.06–0.07 × 10^{-6} S cm^{-1}). All working solutions were prepared by diluting the stock solution with water.

The pharmaceutical sample analyzed was Astymin capsule (Tablets India Ltd., Chennai, India). Human blood serum was collected from a local pathology center and cerebrospinal fluid (CSF) from the Institute of Medical Science, Banaras Hindu University (Varanasi, India). Both samples were kept in a refrigerator at ∼4 °C. Glass capillaries of different internal diameters (0.5, 0.6, 0.7, 0.8, 0.9, 1.0, and 1.2 mm) and micropipette tips were procured from Top-Tech biomedicals (Varanasi, India) and Tarsons products Pvt. Ltd. (Kolkata, India), respectively.

2.2. Apparatus

Voltammetric measurements were carried out with a polarographic analyzer/stripping voltammometer [model 264 A, EG & G Princeton Applied Research (PAR)] in conjunction with an electrode assembly (PAR model 303 A) and *X*–*Y* chart recorder (PAR model RE 0089). Herein a conventional three-electrode system was used where MIP-carbon composite fiber, platinum wire, and saturated Ag/AgCl served as working, auxiliary, and reference electrodes, respectively.

Chronocoulometric measurements were performed with an electrochemical analyzer (CH instruments USA, model 1200 A). IR and ^{1}H NMR characterizations were made by the help of Varian 3100 FT/IR (USA) and JEOL AL 300 FT NMR (Japan) instruments, respectively. Morphological images of MIP-carbon composite were recorded on scanning electron microscope (SEM) (JEOL, JSM, Netherlands, model 840 A). All experiments were carried out at 25 ± 1 °C.

2.3. Preparation of MIP-carbon composite

Monomeric precursor, 4-nitrophenylacrylate (NPA), was prepared following a known recipe [21] by the reaction between NP (25 mmol) and AC (25 mmol) at 0 °C (acetone medium), in the presence of TEA (25 mmol). The preparation protocol of MIP-carbon composite by AGET-ATRP is shown in Scheme 1. Accordingly, bpy (0.02 mmol) and $CuCl_2$ (0.02 mmol) were dissolved in 2 mL DMSO to obtain a solution of Cu (II)-complex. Subsequently, this complex was mixed with NPA (0.2 mmol, 1 mL DMSO), Trp (D or L) (0.1 mmol, 1 mL DMSO), and EGDMA (4 mmol, 1 mL), in the presence of a reducing agent (TEA, 2 mmol, 280 μL). A sharp color change from light blue to brownish yellow indicated an in situ reduction of Cu (II) complex to Cu (I) complex, which catalyzed the chain propagation, in the presence of an initiator (chloroform, 2 mmol, 160 μL). Finally, to this pre-polymer mixture, 120 mg of carbon powder was added and stirred till a slightly viscous and homogeneous solution obtained. The whole content was purged with nitrogen gas for 10 min before pouring into glass capillaries of different diameters (0.5–1.2 mm) with the help of a syringe. Capillary orifices were tightly sealed by teflon tape and kept under strict horizontal position in an oven before curing at 60 °C for 6 h. This helped shaping composite monolithic fibers. The fibers were gently pushed out of capillaries by an insertable wire of diameter just close to that of capillary (Fig. 1A). The withdrawn fibers were washed with methanol and water in order to remove monomer impurity and porogen (DMSO), if any, trapped within the fiber-texture. The templates were retrieved from these fibers by immersing into HOAc–ethanol (9:1, v/v) solution for 40 min, with mechanical stirring of the eluent at 600 rpm until no voltammetric response of the template was observed.

Non-imprinted polymer (NIP)-carbon composite was also prepared as described above but in the absence of the template. In order to study the effect of monomer–template stoichiometry on selectivity of MIPs, we have also synthesized composites taking different molar ratios of template and monomer.

2.4. Sensor fabrication and voltammetric procedure

The prepared MIP fiber was a type of consolidated composite, in which carbon particles have been organized under the action of gravitational force [22]. Majority of carbon particles have been arranged as a strip (visible by naked eye) along the entire length of the fiber (Fig. 1A), and some of theses particles might have dispersed into the polymeric texture.

For the sensor fabrication, 5 mm MIP fiber (diameter 0.8 mm) was inserted in another capillary (6 mm length) which was half-filled with an aqueous agarose solution (0.2 g, 10%, 60 °C). This way only 1 mm length of fiber was fixed inside the agarose (for an easy electrical contact) and remaining 4 mm fiber retained out of the capillary. The capillary was housed with one end in a micropipette tip for safe handling of the extruded fiber; while a copper wire was used at agarose end for the electrical connection (Fig. 1B).

Electrochemical experiments were performed in a cell containing 10 mL PBS (pH 2.0). After blank run, test solution was added in the cell for subsequent measurement. After analyte accumulation for 75 s at −0.2 V vs. Ag/AgCl and 15 s equilibration time, differential pulse anodic stripping voltammograms (DPASV) were recorded in the potential range varying from +0.8 to +1.5 V at a scan rate 10 mV s^{-1}, pulse amplitude 25 mV, and pulse width 50 ms. Cyclic voltammograms (CV) were recorded within the potential window +0.5 to +1.7 V at various scan rates (10–200 mV s^{-1}) in anodic stripping mode. Since oxygen did not influence the oxidation of Trp, the deaeration of cell content was not required. All DPASV runs for each concentration of test analyte were quantified using the

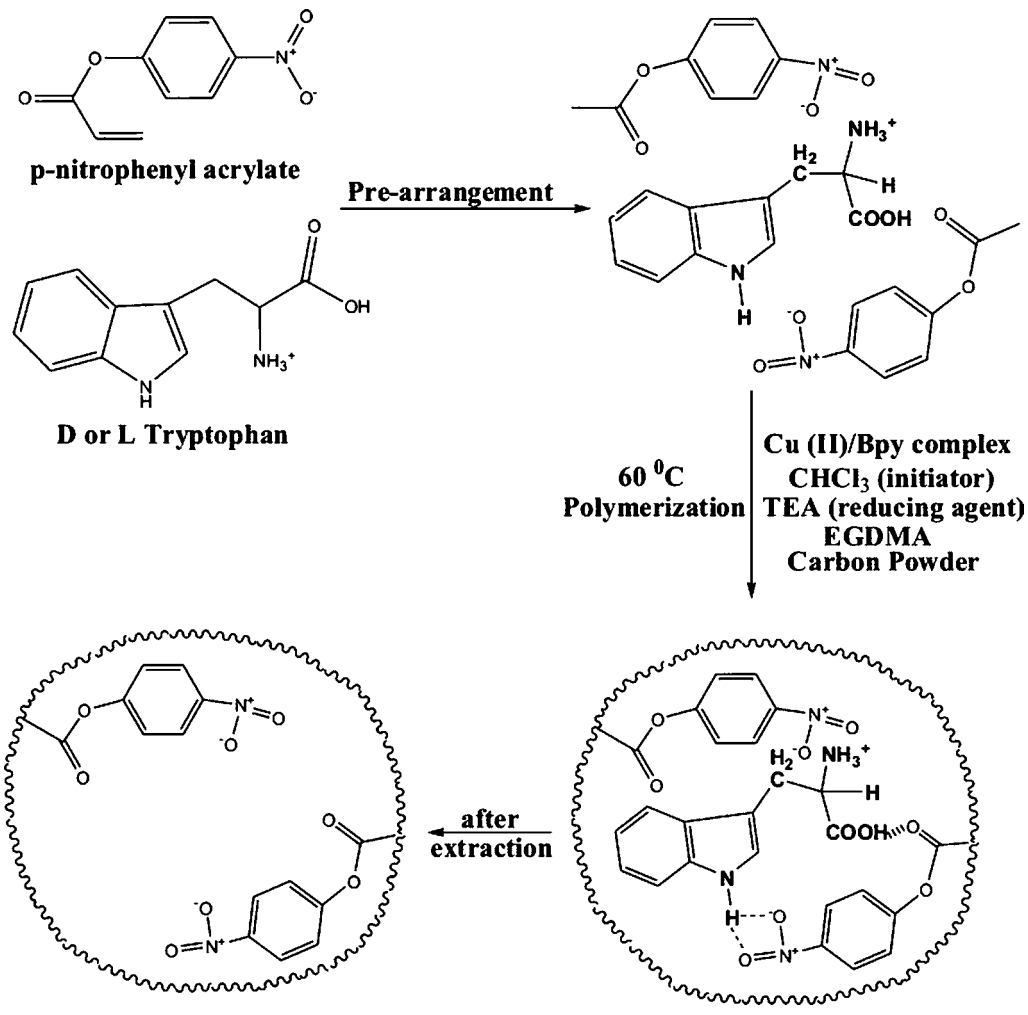

Scheme 1. Schematic representation of the preparation of MIP-carbon composite.

method of standard addition. To demonstrate the MIP-fiber sensor reproducibility, results were averaged for three separately fabricated electrodes and three measurements per electrode. The limit of detection (*LOD*) was calculated as three times the standard deviation from the blank measurement (in the absence of Trp) divided by the slope of calibration plot between Trp concentration and DPASV current [23]. Voltammetric measurements, as mentioned above, were also carried out with NIP-fiber electrodes, under the similar operating conditions.

3. Results and discussion

3.1. Polymer characteristics

MIP-template adducts for D- and L-Trp have similar polymer characteristics, except the difference in the geometrical shapes of molecular cavities in their respective MIPs. Many factors, e.g., polymerization time and polymerization temperature, porogen, polymer composition, thickness, stability (chemical and thermal), and swelling are responsible for specificity in a chiral seletor. Polymerization time affects the composite porosity, since it controls the degree of cross-linkage in a polymeric network. The DPASV current response of the proposed sensor was found to be increased with polymerization time and reached a limiting plateau within six hours. Further, an increase of time (>6 h), results in welding of fiber to the glass capillary. Had it been the duration of polymerization less than one hour, the fiber could not be withdrawn in its shape probably due to less cross-linkage. Thus polymerization time of six hour was optimum for the fiber fabrication. The temperature also played a crucial role in the development of a monolithic fiber. At low temperature (<60 °C), polymerized material required rather more time to be shaped as fiber. On the other hand, given higher temperature (>60 °C) for the chain propagation, polymerization becomes rampant without any control.

Insofar as the selection of porogen is concerted, it is desirable that the solvent used should have high boiling point and be inert under polymerization conditions. Further, to support the effective and homogeneous heating of the polymerizing mixture, especially at the final stages of the process when most of the monomer molecules have been polymerized and have limited mobility, the absorbent of the thermal energy recommended should be a polar solvent [24], like DMSO in the present instance.

The recognition ability of imprinted polymer primarily depends on both the print molecule and functional precursor of the polymer. To study the stoichiometric effect, different template–monomer ratios (1:1, 1:2, 1:3, and 1:4) were investigated and corresponding results are depicted in the Supporting Information (Fig. S1(A)). A few created binding cavities within an MIP, when amount of template is relatively low than that of monomer (say, 1:3 and 1:4), always responded a diminished current owing to the lower adsorption ability of polymer. By increasing the proportionate quantity of template molecules (say, 1:2), the efficiency of prepared polymer fiber sensor has been found to increase as much as to respond an optimum current. However, with further increase of the relative

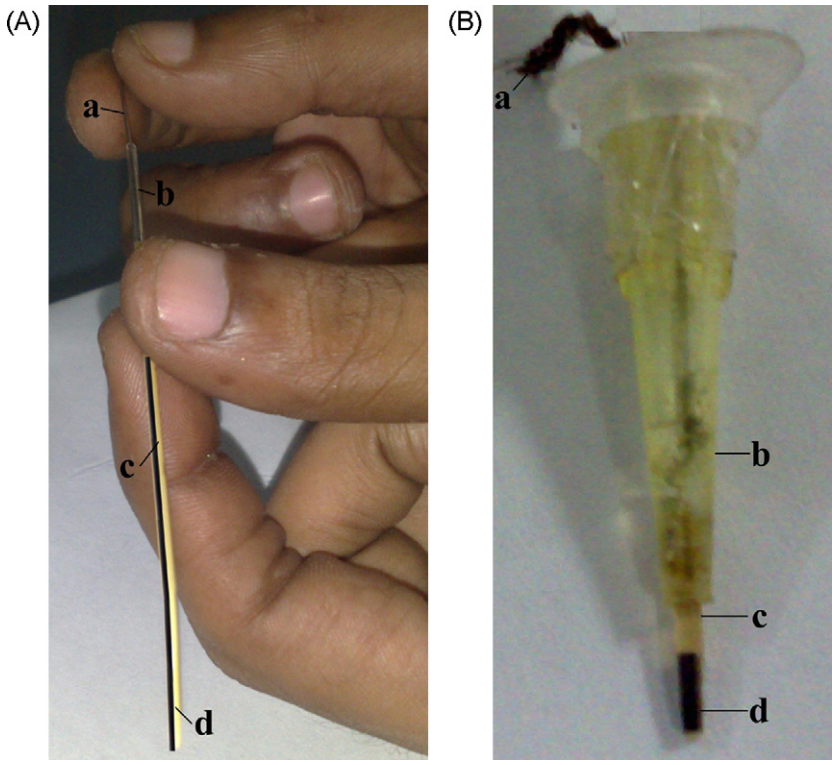

Fig. 1. (A) Picture of MIP-Trp-carbon composite fiber: (a) an insertable wire to push fiber out from the glass capillary, (b) glass capillary, (c) fiber portion inside the capillary, and (d) pushed out fiber embossed with a visible black carbon strip. (B) Picture of fabricated MIP-fiber sensor: (a) copper wire, (b) micropipette tip, (c) agarose solution, and (d) MIP-carbon composite fiber.

concentration of template molecules (say, 1:1), the performance of prepared fiber sensor was decreased, due to an increased heterogeneity, and thereby instability in binding sites. Stoichiometry of the monomer–template complex in this work was calculated on the basis of an empirical equation [25]:

$$\frac{1}{ip} = \frac{1}{ip,\max} + \frac{1}{ip,\max \beta {C_t}^m} \quad (1)$$

where i_p is the measured peak current, $i_{p,\max}$ the peak current when all template molecules formed complex with monomeric precursor, C_t is the concentration of template, m is the coordination number of the complex formed between template and monomer, and β is the stability constant of the complex. Substituting $m = 1$, a perfect straight line ($\nu = 0.895$) of above equation is equivocal; however, $m = 2$ responded a straight line with $\nu = 0.999$, convincing 1:2 composition of the stable template–monomer complex.

Structural integrity of the monomer–template assembly must be preserved during polymerization to obtain well-defined receptor sites in which the functional groups of the monomer are fixed in cooperation with the spatial arrangement of the template. The effect of concentration of the cross-linker on the sensitivity of MIP-carbon composite fiber was also evaluated (Fig. S1(B)). Accordingly, the DPASV current was increased for the sensor fabricated with 1:15 molar ratio of monomer and EGDMA, owing to an improved stabilization of binding sites. Further increase of cross-linker led to a decrease in current response due to the formation of excessively cross-linked domains in MIP matrix providing relatively a poor access to the template.

Electrical conductivity of MIP-carbon composite basically depends on the carbon content present in its matrix. The carbon content governs the morphology of composite which in turn affect the DPASV current response (Fig S1(C)). The current response was observed to be increasing with the increase of carbon content up to 120 mg and then decreased either due to restricted permeability through denser matrix or due to decrease of the recognition element on the electrode.

The influence of fiber thickness on DPASV current response of Trp (D or L) was also evaluated (Fig. S1(D)). As expected, current response was found to be increased with the fiber thickness up to 0.8 mm, and then assumed a constant response owing to the saturation of binding sites. For a better comprehension, in the present case, the area and volume of cylindrical fiber are also to be accounted as additional factors to affect the current response. A linear relationship between current and volume (or area):

$$I_p\,(\mu A) = (42.14 \pm 2.89)\,\text{volume} - (11.81 \pm 4.16), \quad \nu = 0.99 \quad (2)$$

$$I_p(\mu A) = (11.85 \pm 0.47)\text{area} - (59.05 \pm 4.27), \quad \nu = 0.99 \quad (3)$$

exists with the fiber sensors. This indicated that template molecules had unhindered access, also to all those binding sites which were located deep inside the fiber, owing to its porous structure.

Thermogravimetric study in the thermal range of 60–410 °C in the stream of inert gas (argon) revealed that composite could withstand up to 380 °C without any damage to the material. To examine chemical stability of the composite, fibers were immersed in methanol, TEA, HCl (pH 1.0), and NaOH (pH 12.0), separately for 24 h at 25 °C. These composite fibers were then used as electrode which revealed no variations in DPASV current response.

Swelling ratio was determined for bulk MIP and NIP particles (40–50 μm, estimated by a particle size analyzer, Microtrac Inc., USA) in different solutions based on the method described by Feás et al. [26]. The swelling ratio (S_r) was calculated using equation:

$$Sr(\%) = \left[\frac{ms - mo}{mo}\right] \times 100 \quad (4)$$

where m_s the mass of the swollen polymer and m_o is the mass of the dry polymer. Swell data (vide supporting information, Table S1) indicates that there is a fast increase in degree of swelling with the slight decrease of the amount of cross-linker. This implies that low-

ering EGDMA contents, solvent has initially a higher rate of ingress into the polymer formed, owing to its more flexible nature. Consequently, the higher swelling of the polymer network with the decrease of cross-linkage, as was in the case of MIP formed with 10 mmol EGDMA, has responded a diminished DPASV current probably due to the severe distortion of binding sites [27]. Therefore, a critical amount of EGDMA to be used in MIP synthesis was 15 mmol which responded quantitative response of Trp binding in aqueous medium. The swelling of NIP had no impact on analyte binding as it was found to be non-responsive to analyte at any concentration studied. The larger extent of swelling of the MIP in Trp-water, which allowed maximum binding of Trp, supports the higher affinity for analyte rebinding in aqueous medium in comparison to porogen (DMSO) used in MIP preparation.

3.2. SEM analysis

SEM images can provide information about the morphological structure and distribution of carbon particles within the composite. Fig. 2A shows SEM images of MIP-Trp-carbon composite at low magnification (50×). The composite fiber surface is heterogeneous, with polymer zone in lighter area and conducting zone of carbon particles in darker area; some of the carbon particles have been interspersed within the polymer zone. The distribution of carbon particles in well-organized manner as a strip, adhered to the full length of prepared fiber can be seen by naked eye. The microporous characteristics of such composite fiber, after template retrieval, can be visualized in Fig. 2B. However, at high magnification (6000×), MIP-Trp-carbon composite (Fig. 2C) showed

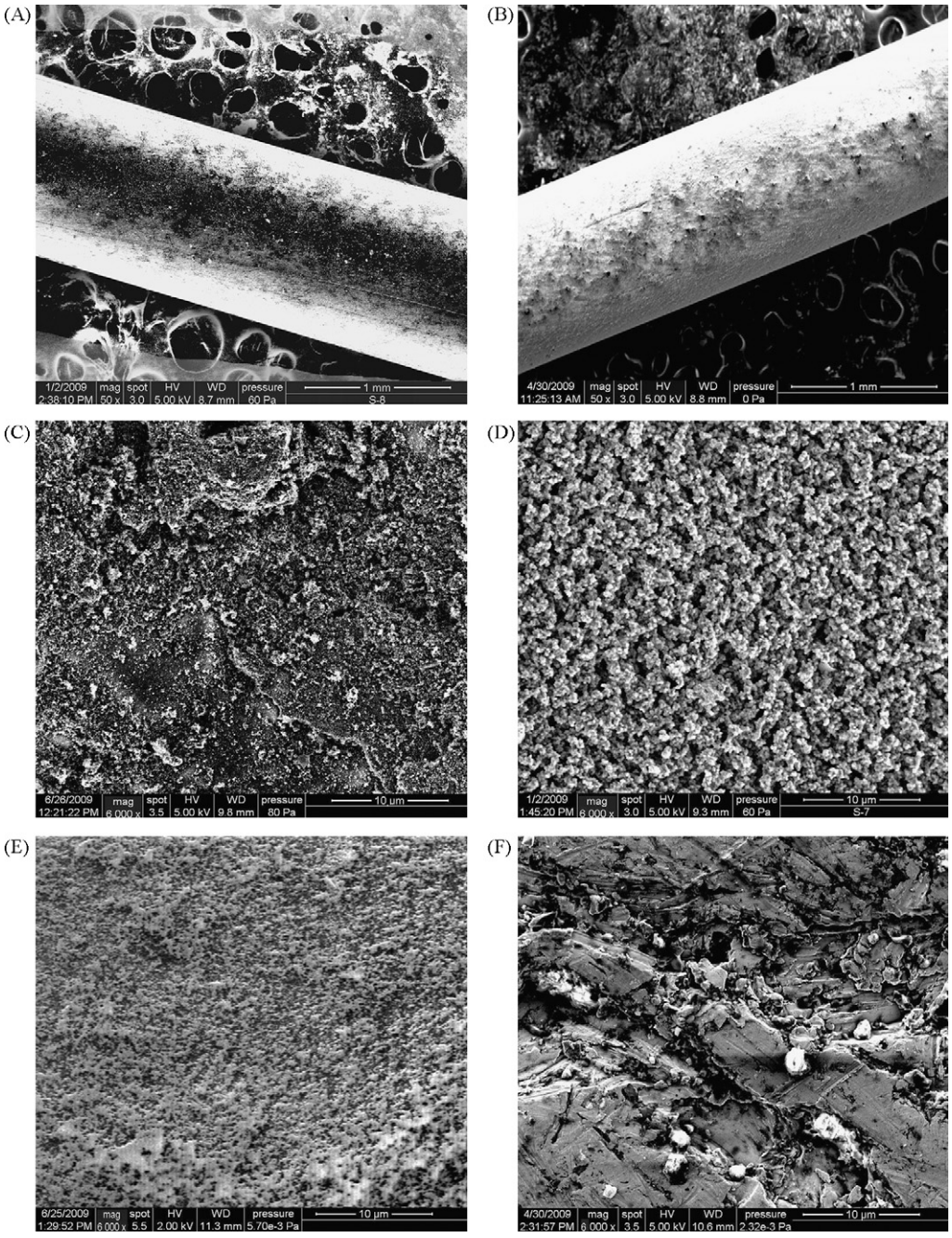

Fig. 2. SEM images of MIP-Trp-carbon composite fiber: (A) 50×, 120 mg carbon, (C) 6000×, 120 mg carbon, (E) 6000×, 90 mg carbon, and (F) 6000×, 150 mg carbon. SEM images, B and D, represent MIP-carbon composite fiber (120 mg carbon) at magnifications 50× and 6000×, respectively.

some compactness, which later, after template removal, turned microporous with interconnected penetrable texture (Fig. 2D). The uniform distribution of pores (Fig. 2D) was possible at the behest of living polymerization that led a better homogeneity towards binding sites. The fibers shown in SEM images (Fig. 2A–D) have 120 mg carbon particles. Any amount lesser than this may result in a relatively thin carbon pack or low dispersed carbon particles in polymer matrix (Fig. 2E), which was found insufficient to inculcate electrical conductivity to respond optimum current. On the other hand, increasing the carbon content led to an easily breakable deformed electrode surface (Fig. 2F), and thereby decreased MIP content.

3.3. Spectral characterization and recognition mechanism in aqueous medium

FT-IR spectra (Fig. 3) of template (curve A), MIP-Trp adduct (curve B), and MIP (curve C) are compared to study binding mechanism in the porogen (DMSO). The rebinding interactions of Trp (D or L) with MIP binding sites in aqueous medium (curve D) have also been studied to explore water-compatible characteristics of the proposed MIP fiber. Interestingly, the template (Trp) possesses both hydrophobic (due to indole ring) and hydrophilic (due to amino and carboxyl group) characteristics. These characteristics ought to be present in the host (MIP) too for an effective binding of the template within its cavity. In the present instance, the hydrophobic phenyl constituents of the MIP thus involved π–π interaction with the hydrophobic Trp-indole ring as suggested by downward shifting of bands from 1672, 1534, and 1492 cm^{-1} (curve A) to the respective lower wave numbers 1592, 1500, and 1408 cm^{-1} (curve B). In the similar tune, downward shifting in stretching bands (3117–2600 cm^{-1}, curve A) of hydrophilic $-NH_3^+$ (Trp) and that (ν_{as} 1692 and ν_s 1343 cm^{-1}, curve C) of $-NO_2$ group (MIP) after MIP-Trp adduct formation (cf, curve B) suggest, an ion-pair association between $-NH_3^+$ and resonance stabilized negatively charged $-NO_2$ group (host). Further, the downward shifts of 3484 cm^{-1} (–COOH stretching of Trp, curve A) and 1774 cm^{-1} (MIP ⟩C=O, curve C) to 3432 and 1720 cm^{-1} (curve B), respectively, attribute hydrogen bonding between –COOH (guest) and ⟩C=O (host) groups. Indole –NH is also involved an interaction with $-NO_2$ group of the polymer via hydrogen bond, causing downward shifts from 690, 586, and 507 cm^{-1} (curve A) to 640, 550, and 480 cm^{-1} (curve B), respectively. It is to be noted that all shifted bands (curve B) of MIP-Trp adduct reassumed their original positions on template retrieval and appeared sharper (curve C). The template bands, which were found disappeared (curve C) in MIP, were reinstated at the same position with similar magnitude after rebinding in aqueous medium. When applying the MIP in water systems, the concerted actions of several interaction forces, as mentioned above, in non-aqueous environment may overcome the water influence. Despite the fact that the strong influence of water in disrupting weak hydrogen bonds, the ionic as well as hydrogen bonds in the present case (Scheme 1) are potent enough to persist in aqueous media. This substantiates the water compatibility of the proposed MIP system [28].

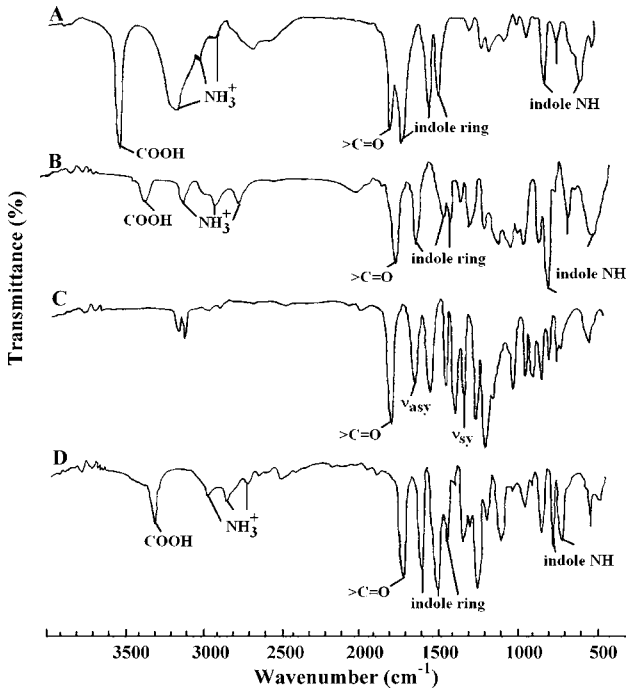

Fig. 3. FT-IR (KBr) spectra of (A) template (D- or L-Trp), (B) MIP-Trp-carbon composite, (C) MIP-carbon composite, and (D) Trp rebinding into MIP cavities in the aqueous environment.

The proton NMR also corroborated binding interactions as follows: all Trp (D or L) peaks 11.0 (–COOH), 10.1 (indole –NH), 7.2 ($-NH_3^+$), and 7.18 ppm (ring protons) were shifted downfield to 11.5, 10.5, 7.6, and 7.2 ppm, respectively, after binding with MIP. Like IR, these peaks were simultaneously appeared and disappeared after sorption and desorption, respectively; major peaks [7.5–8.5 ppm (aromatic protons) and 1.5–3.35 ppm ($-CH_2$ and –CH)] pertaining to MIP backbone were retained unaltered.

3.4. Electrochemical behavior

Since entire perimeter of the fiber surface, including its inner cross-section, was utilized for analyte uptake, the mass-transport in the present instance was basically a non-linear diffusion which resulted in current response with higher signal-to-noise ratio. This could be the reason that residual currents obtained in this work were free from any distinguishable noise [29] (Fig. 4A–C, run 1). The CV runs of Trp in anodic stripping mode at various scan rates (ν = 10–200 mV s^{-1}) were shown in Fig. 4A. Before voltammetric measurement, the MIP-carbon composite electrode was first activated and made cathodic in PBS (pH 2.0) at −0.2 V vs. Ag/AgCl (accumulation potential, E_{acc}). At this potential, the analyte was accumulated for 75 s (accumulation time, t_{acc}). The analyte recapture in MIP cavity was apparently facilitated by an electrostatic force between positively charged analyte and negatively charged electrode and mainly by MIP-template interaction as shown in Scheme 1. The entrapped Trp molecules were desorbed (stripped) anodicaly under electrostatic repulsion accompanying the corresponding oxidative peaks based on the known irreversible oxidation ($2e^-$, $2H^+$) mechanism [30]. The weak adsorption of the oxidation product at the electrode surface may be concluded from the appearance of a pre-peak at fast scan rate of 200 mV s^{-1}, due to the limited time available for stripping. However, the oxidation peak potential (E_{pa}) was found to be positively shifted with scan rate and the peak current (I_{pa}) increased linearly with increase of scan rate as depicted below:

$$E_{pa}\,(V) = (0.151 \pm 0.004)\log \nu + (1.052 \pm 0.007),\ \nu = 0.99 \quad (5)$$

$$I_{pa}\,(\mu A) = (1.09 \pm 0.09)\nu + (13.39 \pm 5.50),\ \nu = 0.99 \quad (6)$$

This may be attributed to the strong adsorption of Trp in the binding cavities of MIP-fiber sensor which resulted in somewhat sluggish stripping with the drawn out anodic peak. Herein the adsorbed species may attain an equilibrium, $Trp_{(adsorbed)} \leftrightarrow Trp_{(dissolved)}$, within the sufficient time span (scan rate 10 mV s^{-1}) and there is basically, no difference in energy between both type of species to give rise to a post-anodic peak. Thus a diffusion-controlled irreversible oxidation of Trp molecules occurred in the anodic stripping mode. A linear equation between

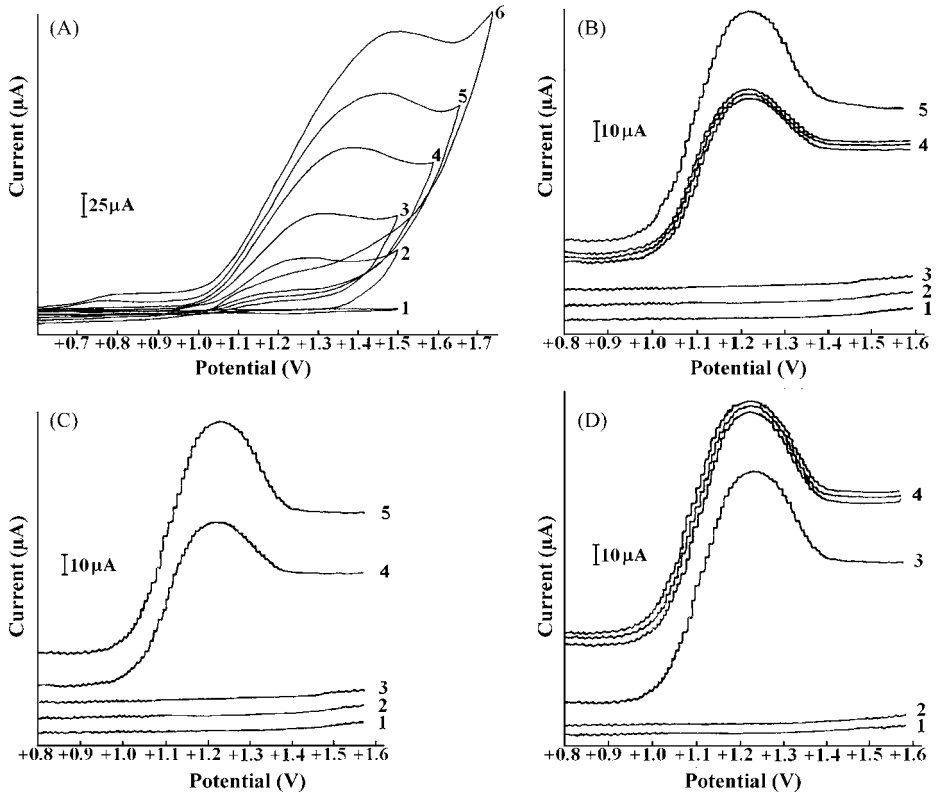

Fig. 4. (A) CV runs (anodic stripping) of 500 ng mL^{-1} L-Trp on MIP-carbon composite fiber (electrode 1, 120 mg carbon) at different scan rates: (1) blank, 10, (2) 10, (3) 20, (4) 50, (5) 100, and (6) 200 mV s^{-1} (optimized operating conditions: E_{acc} −0.2 V vs. Ag/AgCl, t_{acc} 75 s, pH 2.0). (B) DPASV response on MIP-carbon composite fiber (electrode 1, imprinted for L-Trp) sensor: (1) blank, (3) D-Trp (16.49 ng mL^{-1}), (4) L-Trp (7.5 ng mL^{-1}), and (5) L- and D-Trp mixture (both 11.0 ng mL^{-1}). (C) DPASV response of MIP-carbon composite fiber (electrode 2, imprinted for D-Trp) sensor: (1) blank, (3) L-Trp (16.49 ng mL^{-1}), (4) D-Trp (7.5 ng mL^{-1}), and (5) L- and D-Trp mixture (both 11.0 ng mL^{-1}). (D) DPASV response on electrode 1 for 11.0 ng mL^{-1} L-Trp in CSF (run 3) and blood serum (run 4). DPASV response of 11.0 ng mL^{-1} Trp on NIP-carbon composite fiber sensor: B-C, run 2 (aqueous) for L- and D-Trp, respectively; (D) runs 1 and 2 for L-Trp in CSF and blood serum sample, respectively.

the anodic stripping current (I_{pa}) and square root of scan rate ($v^{1/2}$):

$$I_{pa}\,(\mu A) = (14.78 \pm 0.17)\,v^{1/2} + (-28.51 \pm 1.20), \quad \nu = 0.99 \qquad (7)$$

supported the fact that the stripping process was actually a diffusion-controlled phenomenon. The heterogeneous charge transport might occur from the redox centers located in polymer zone to the carbon strip on anodic scan apparently with a faster kinetics, without any diffusion barrier. We have calculated the standard heterogeneous rate constant (k_s) for the irreversible oxidation of the stripped Trp molecules from the MIP-carbon fiber electrode by applying CV data in the following equations [31]:

$$\alpha\, n = \frac{1.857RT}{F(Epa - Epa/2)} \qquad (8)$$

$$Epa = Epa/2 - b\left[0.52 - 0.5\log\left(\frac{b}{D}\right) - \log k_s + 0.5\,\log v\right] \qquad (9)$$

$$b = \frac{2.303RT}{\alpha\, nF} \qquad (10)$$

where α = transfer coefficient, E_{pa} = peak potential, $E_{pa/2}$ = half peak potential, b = tafel coefficient, D = diffusion coefficient, and v = scan rate; other parameters have their usual meanings. In order to determine the k_s, it is necessary to find the 'D' of Trp. The D value was determined by chronocoulometric technique involving charge (Q) versus square root of time ($t^{1/2}$) plot for the Anson equation [32]:

$$Q = 2nFAC(Dt)^{1/2}\,\pi^{-1/2} + Q_{ads} + Q_{dl} \qquad (11)$$

$$Q_{ads} = n\,F\,A\,\Gamma^0 \qquad (12)$$

where A is the area of electrode (0.11 cm^2), C is the concentration of analyte (500 ng mL^{-1}), Q_{dl} is the double layer charge, Q_{ads} is faradic oxidative charge and Γ^0 is the surface coverage. The slope thus obtained (5.86×10^{-4} μC s^{-1}) revealed an estimate of 9.23×10^{-5} cm^2 s^{-1} for the parameter D. The intercept of the plot tantamount to the total charge ($Q_{dl} + Q_{ads}$) of 8.64×10^{-5} μC; the value of Q_{dl} was estimated by the similar plot but in the absence of analyte. On subtraction of Q_{dl} from the total charge, Q_{ads} was obtained to be 0.842 μC. The value of Γ^0 can be obtained in terms of the number of electrons (n) from the following empirical equation [33] defining Nerstian adsorbate layer:

$$Ipc = \left[\frac{n^2F^2}{4RT}\right]\Gamma^0 A\nu \qquad (13)$$

The values of n and Γ^0 can be obtained as 2.08 and 3.94×10^{-9} mol cm^{-2}, respectively. In the present instance, Γ^0 reflects the total surface coverage of Trp analyte (0.435×10^{-9} mol or 2.62×10^{14} molecules) specifically bound to MIP cavities (each molecule per cavity). The estimated α and k_s values (from Eqs. (8)–(10)) for the oxidation of Trp at MIP-carbon composite electrode were found to be 0.20 and 1.48×10^{-2} cm s^{-1}, respectively. It is to note that electrode transfer kinetics of Trp at the electrode surface is still ambiguous. The general observation is that the voltammetric response of Trp is not satisfactory due to the slow heterogeneous electron-transfer rate at the electrode surface [30]. Nevertheless, the higher D and k_s values in this investigation are considerable to implement non-linear homogeneous mass-transfer across the perimeter of cylindrical fiber and heterogeneous electron transfer from interior to exterior electrode surface for obtaining better and quantifiable current response. Insofar as sensitivity of the measurement is concerned, the DPASV technique is better than CV at the scan rate 10 mV s^{-1} because differential pulse modulation

amplitude (25 mV) and pulse width (50 ms) help to obtain higher current in the sufficient time scale of the measurement. As can be seen in DPASV runs (Fig. 4B and C), MIP-carbon composites for L-Trp (electrode 1) and D-Trp (electrode 2) were found responsive exclusively for their respective templates. Electrode 1 was not responsive for D-Trp (Fig. 4B, run 3), but responsive for L-Trp, either examined alone (Fig. 4B, run 4) or in binary mixture of D- and L-Trp (Fig. 4B, run 5). Similarly, Electrode 2 was found to be responsive for D-Trp either alone (Fig. 4C, run 4) or in racemic mixture (Fig. 4B, run 5), and not responsive for L-Trp (Fig. 4C, run 3) at any concentration studied. This reflects the excellent selectivity with composite fiber electrodes by the virtue of imprinting effect created in the polymer composite. As a matter of fact the proposed NIP-fiber sensors did not respond the test analyte at any concentration in aqueous and real samples (Fig. 4B–D). Although carbon particles can physically adsorb some template molecules, their presence in this work did not reveal any non-specific (physical) adsorption of the template with MIP/NIP-fiber sensors. This may be attributed to the relatively low amount of carbon particles which were only sufficient to impart electrical conduction. This suggests that DPASV response with MIP-fiber sensor is free from any non-specific contribution. The probable matrix complications, protein interference in particular, from blood serum and CSF samples were not effective as can be seen from the quantitative DPASV response of L-Trp in these samples (Fig. 4D).

3.5. Optimization of analytical parameters

Operating conditions for DPASV measurements were optimized for E_{acc}, t_{acc}, and the solution pH. As suggested from Fig. S2(A) in the supporting information, the optimum accumulation potential was −0.2 V vs. Ag/AgCl for analyte accumulation under electrostatic forces; any potential lesser or higher than this may cause instability to MIP structure (owing to the reduction of nitro to amino group) [34] and electrostatic repulsion (between Trp cation and positively charged electrode), respectively. For all DPASV runs, t_{acc} used was 75 s; after this saturation in binding sites responding constant DPASV current was observed. The supporting electrolyte pH had major impact on the oxidation of Trp (Fig. S2(B)). Accordingly, the maximum development of DPASV current was reached at pH 2.0; any pH higher than this revealed a sharp fall in current owing to the deprotonation of Trp $-NH_3^+$ as well as –COOH groups (pK_1 2.38, pK_2 9.39) which caused an instant desorption of Trp from binding sites under electrostatic repulsion. The peak potential (E_p) was found to shift negatively following a linear equation:

$$E_p\,(V) = (-0.057 \pm 0.007)\mathrm{pH} + (1.345 \pm 0.029), \quad \nu = 0.98 \quad (14)$$

The slope of the above equation corroborates the involvement of equal number of electron and proton ($2e^-$, $2H^+$) taking part in the electrode reaction [30].

3.6. Determination of Trp

MIP-carbon composite electrodes were employed for the DPASV determination of Trp. Analytical data obtained from electrodes 1 and 2 are summarized in Table 1. Both electrodes revealed almost equal current and quantitative recovery of their respective template analyte of known concentration. In view of the clinical significance of L-Trp determination as a disease biomarker, electrode 1 was subjected to extensive investigation and the corresponding results are portrayed in Table 2. Accordingly DPASV peak current (I_p) was found to be proportional to the concentration (C) of L-Trp over two concentration intervals viz. 0.90–18.60 ng mL^{-1} and 24.23–840.22 ng mL^{-1} of aqueous samples. The earlier saturation of current above 18.60 ng mL^{-1} in the lower concentration region may be taken as manifestation of highly favored multiple interactions between guest and host. The constant current response in the range of 18.60–24.23 ng mL^{-1} may be attributed to the saturation of binding sites irrespective of analyte concentration; and therefore, this concentration interval does not favor accurate L-Trp analysis from the linear regression equations (Table 2) obtained for both ranges of concentration. However, if the concentration of L-Trp is just in the range of 18.60–24.23 ng mL^{-1}, it could be analyzed by moving the analyte concentration to the concentration range of linear regression equations (Table 2) either by dilution or standard addition method. The binding site saturation was not implicated with a new set of experiment performed on a fresh sensor in the higher concentration range of analyte. Under such condition, throughout the concentration range of analyte some restriction might occur in its mass-transfer (diffusion) from bulk to the electrode owing to the formation of hydrophobic clusters of Trp molecules. The large indole ring of Trp is reportedly known to participate in the formation of non-polar clusters and also in intermolecular hydrogen bonding [35]. Consequently, the relative magnitude of DPASV current and slope of corresponding linear regression equation were curtailed by 25-fold as compared to those of lower concentration region. Nevertheless, the observed linearity between I_p and C in the higher concentration region with the correlation coefficient (ν) 0.9998 (Table 2) may be opted for the accurate analysis of L-Trp. The proposed sensor is compared with a known electrode (multiwalled carbon nanotube modified carbon paste electrode) with differential pulse voltammetry sensing [36], by means of Student's t-test [t_{cal} (2.00) < t_{tab} (2.57), confidence level 95%]. Although both methods have similar order of precision within the concentration range (24.23–840.22 ng mL^{-1}) studied, the proposed MIP-fiber sensor is at least 20 times more sensitive than the known method (*LOD* 20.40 ng mL^{-1}).

The life span of sensor is important as it determines the cost, accuracy, and repeatability of analysis. The proposed sensor was found reusable, after template removal for as many as 90 consecutive DPASV runs, with no deterioration in its sensing capability. It was affected with decreasing recoveries of test analyte only after (i) 91, (ii) 92, and (iii) 95 consecutive runs by the same electrode regenerated on every alternate day (Table 1). The reproducibility of the method in DPASV measurement on a single fiber sensor, regenerated after each run, was confirmed by multiple DPASV runs (Fig. 4B and D, run 4) for Trp concentration 7.50 and 11.00 ng mL^{-1} in aqueous and blood samples, respectively. With respect to electrode-to-electrode variation, all DPASV measurements revealed a high degree of precision (*RSD* 1.3%, n = 3) with quantitative recovery of Trp concentration (16.49 ng mL^{-1}, Table 1) achieved with each electrode in the present instance. The maximum *RSD* in intra-day assay for the different concentrations of Trp in aqueous samples may reach up to 3.7% which is accepted for any practical application (Table 1).

The method validity in the present work was examined for real samples. In view of the fact that no non-specific (false-positive) contribution was observed in biological fluids analysis (human serum and CSF), their preliminary treatment (deproteination, ultrafiltration, ultracentrifugation, etc.) was not required. Although dilution of biological fluids of the patients suffering from acute Trp deficient diseases is not required, this appeared inevitable for control samples [dilution factor 2500 (serum), 500 (CSF)] of healthy person so as to move the analysis to within the linear range of trace-level detection and to realize the actual detection limit (0.24 ng mL^{-1}) by sensor. Such heavy dilutions have no impact on the accuracy of results and ruggedness of the fiber sensors as their behavior assumed similar to that of aqueous samples (cf. calibration equations, Table 2); in all cases quantitative (100%) recoveries, without any non-specific contribution and matrix interferences were obtained. The pharmaceutical capsule analyzed by the proposed sensor had similar characteristics with *LOD* 0.24 ng mL^{-1}.

Table 1
Analytical results of DPASV measurements on MIP-carbon composite fiber (electrode 1) imprinted for L-Trp and MIP-carbon composite fiber (electrode 2) imprinted for D-Trp in aqueous samples.

Concentration (ng mL^{-1})	Response of electrode 1				Response of electrode 2			
	Analyte	I_p (μA)	Recovery (%)	*RSD* (%) ($n=3$)	Analyte	I_p (μA)	Recovery (%)	*RSD* (%) ($n=3$)
0.90	L-Trp	6.0	100.3	3.7	D-Trp	6.25	100.2	3.2
3.23	L-Trp	21.0	100.3	2.9	D-Trp	20.75	100.0	2.6
9.76	L-Trp	60.0	100.2 [98.0 (i), 96.0 (ii), 90.0 (iii)][a]	1.3	D-Trp	60.5	100.3	1.8
16.49	L-Trp	100.0	99.6	1.3	D-Trp	100.25	99.8	1.6
18.63	L-Trp	112.5	101.1	3.3	D-Trp	112.0	100.9	2.2
16.49	D-Trp	No current	–	–	L-Trp	No current	–	–
7.5	Both D & L	47.0	100.7	3.2	Both D & L	47.25	99.6	3.0

[a] Recoveries after (i) 91, (ii) 92, (iii) 95 consecutive runs recorded by same electrode regenerated at every alternate day.

Table 2
Sample behavior.

Sample	Regression equation	Correlation coefficient (ν)	Range (ng mL^{-1})	Recovery (%)	*LOD* [a] (3σ) ($n=3$)	*RSD*[b] (%) ($n=3$)
Aqueous (lower range)	$I_p = (5.960 \pm 0.024)\,C + (1.631 \pm 0.273)$, $n=11$	0.9999	0.9–18.6	99.6–102.3	0.240	1.2
Aqueous (higher range)	$I_p = (0.234 \pm 0.002)\,C + (2.932 \pm 0.821)$, $n=11$	0.9998	24.23–840.2	99.2–101.3	–	–
Blood (2500 times diluted)	$I_p = (6.382 \pm 0.012)\,C + (0.645 \pm 0.138)$, $n=10$	0.9999	0.92–17.2	99.0–101.6	0.241	1.4
CSF (500 times diluted)	$I_p = (6.133 \pm 0.025)\,C + (0.957 \pm 0.302)$, $n=9$	0.9999	1.1–15.2	99.4–101.6	0.245	1.1
Capsule (lower range)	$I_p = (6.225 \pm 0.016)\,C + (0.794 \pm 0.151)$, $n=9$	0.9999	0.9–14.9	99.4–101.0	0.240	1.8
Capsule (higher range)	$I_p = (0.230 \pm 0.002)\,C + (2.598 \pm 0.644)$, $n=8$	0.9998	123.5–584.4	99.6–101.3	–	–

[a] *LOD* based on the minimum distinguishable signal for lower concentration of analyte.
[b] *RSD* (%) for three sets of *LOD* data.

3.7. Enantioselectivity and cross-reactivity

The difficulty in achieving selectivity for enantiomer molecules follows that the enantiomer molecules differ only in the three-dimensional geometry of the constituent atoms in space, while the remaining properties of both molecules are identical. The enantiodifferentiation of the sensor signal requires the interaction of the determined chiral compound (one or a mixture of enantiomers) and a selector. This interaction is controlled by at least three binding centers, whose mutual arrangement and characteristics of interactions with one of the enantiomers control the selectivity of recognition. The use of enantiomer in the present work, at the step of pore formation in MIP, allowed the development of homogeneous binding sites that specifically extracted an optical isomer from a solution in the quantitative manner. The template molecule interacted at its three points, i.e., cationic

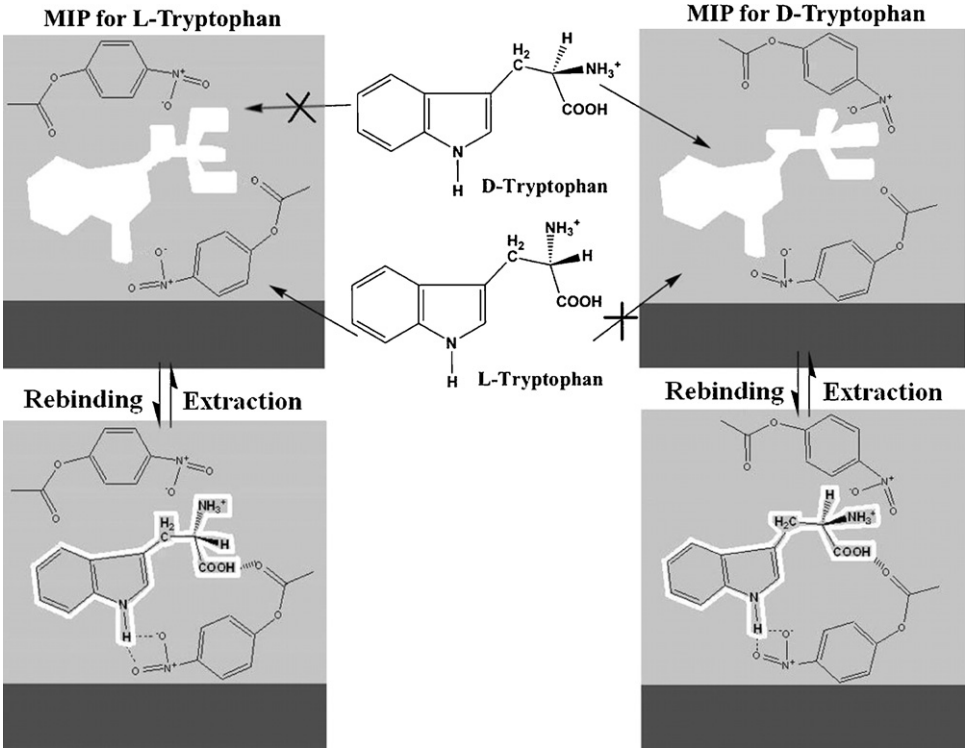

Fig. 5. Enantioselective binding of D- and L-Trp in molecular cavities of their respective MIPs (carbon particles are assimilated to MIP fiber as a black strip).

part (NH_3^+), carboxylic group, and indole ring to the MIP fiber. As is evident from Fig. 5, cavities created in MIP formats were very specific for their respective templates; the rebinding of L-Trp occurred rapidly to the shape imprinted cavity, but D-Trp could not favorably enter into the L-Trp imprinted cavity, primarily due to shape and functional group mediated constraints. The reverse is the case with D-Trp imprinted polymer. The result being, that the imprinted Trp processes a good capability to enantioselectivity recognize D- and L-Trp molecules, at optimized operation conditions of DPASV operation. The major part played toward enantioselectivity was primarily due to the delocalized lone pair electrons of $-NO_2$ group (resonance stabilized) in the receptor network which could exert an electrostatic interaction with cationic ($-NH_3^+$) functionality of the template understudy. Both functionalities (p-orbital lone pair electrons of $-NO_2$ and $-NH_3^+$ group) involved spatial complementarities toward the electrostatic interaction in a plane perpendicular to the molecular planes of receptor/template, depending on the structural configurations of D and L isomers.

Cross-selectivity of amino acids (cysteine, tyrosine, histidine, glycine, cystine, and phenylalanine), ascorbic acid, and 3-indole acetic acid were also studied. Of all, tyrosine has been found to interfere extensively with Trp detection in many instances reported earlier [37]. However, the present sensor did not reveal DPASV peak for individual interferent or mixture of interferents (Table S2). Despite being structural analogues of Trp, tyrosine and 3-indole acetic acid had no binding affinity with the MIP-fiber sensor presumably due to the absence of indole ring in tyrosine and $-NH_3^+$ group in 3-indole acetic acid. This supports that the molecular recognition is feasible only when the necessary and sufficient condition of minimum three-point interaction between MIP and template is followed in this study. Insofar as investigation related to binary mixture of template and interferents (clinically relevant concentration ratio, 1:10) are concerned a highly selective and quantitative analysis of L-Trp was observed with MIP-fiber sensor, without any interference.

4. Conclusions

The described MIP-carbon composite fiber sensor has shown an unique enantioselective feature for the trace-level analysis of D- and L-Trp. For this a shape complementry cavity in the composite was created by AGET-ATRP method. The fiber-texture of MIP-carbon composite, favored non-linear diffusion of target analyte around its cylindrical shape both at surface and inside the MIP matrix. The binding mechanism involved typically three-point non-covalent interactions (electrostatic and hydrogen bonding) between the analyte and MIP, which disallowed non-specific bindings of structural analogues and potential interferents. The developed sensor can easily be regenerated for next uses maintaining enantioselective ability to discriminate D- and L-Trp. The L-Trp imprinted MIP-fiber sensor responded quantitative DPASV peak of L-Trp without any cross-recativity with the D-Trp, interferents, and matrices of real samples. The trace-level analysis of L-Trp, without false-positives, in biological fluids has practical application in clinical setting, particularly as 'disease biomarker'.

Acknowledgments

Authors thank Council of Scientific and Industrial Research, New Delhi for the award of a junior research fellowship (to R.M.). Instrumental facility by the Department of Science and Technology, through project SR/S1/IC-18/2006, is gratefully acknowledged.

Appendix A. Supplementary data

Supplementary data associated with this article can be found, in the online version, at doi:10.1016/j.talanta.2009.11.055.

References

[1] S. Ahuja, Chiral separations by liquid chromatography, in: ACS Symp. Ser, Am. Chem. Soc., Wachington, DC, 1991.
[2] Z. Wang, G. Luo, J. Chen, S. Xiao, Y. Wang, Electrophoresis 24 (2003) 4181–4188.
[3] M.G. Finn, Chirality 14 (2002) 534–540.
[4] L. Zhu, S.H. Shabbir, E.V. Anslyn, Chem. Eur. J. 13 (2006) 99–104.
[5] Z.-B. Li, J. Lin, Y.-C. Qin, L. Pu, Org. Lett. 7 (2005) 3441–3444.
[6] C. Wolf, S. Liu, B.C. Reinhardt, Chem. Commun. 40 (2006) 4242–4244.
[7] L. Zhang, M. Song, Q. Tian, S. Min, Sep. Purif. Technol. 55 (2007) 1182–1188.
[8] H.-J. Liang, T.-R. Ling, J.F. Rick, T.-C. Chou, Anal. Chim. Acta 542 (2005) 83–89.
[9] B. Deore, Z. Chen, T. Nagaoka, Anal. Chem. 72 (2000) 3989–3994.
[10] H. Okuno, T. Kitano, H. Yakabe, M. Kishimoto, B.A. Deore, Anal. Chem. 74 (2002) 4184–4190.
[11] P. Andrea, S. Miroslav, S. Silvia, M. Stanislav, Sens. Actuators, B 76 (2001) 286–294.
[12] M.C. Blanco-López, L. Fernández-Llano, M.J. Lobo-Castañó, A.J. Miranda-Ordieres, P. Tuñón-Blanco, Anal. Lett. 37 (2005) 915–927.
[13] H.U. Tang, M. Radosz, Y. Shen, Macromol. Rapid Commun. 27 (2006) 1127–1131.
[14] M. Bompart, K. Haupt, Aust. J. Chem. 62 (2009) 751–761.
[15] W. Kochen, H. Steinhart (Eds.), L-Tryptophan: Current Prospects in Medicine and Drug Safety, Walter de Gruyter, Berlin/New York, 1994.
[16] I. González-Burgos, E. Olvera-cortés, A.R. Del Angel-Meza, A. Feria-Velasco, Neurosci. Lett. 190 (1995) 143–145.
[17] L.F.B. Malta, Y. Cordeiro, L.W. Tinoco, C.C. Campos, M.E. Medeiros, O.A.C. Antunes, Tetrahedron: Assym. 19 (2008) 1182–1188.
[18] Y. Liao, W. Wang, B. Wang, Bioorg. Chem. 26 (1998) 309–322.
[19] F. Liu, X. Liu, S.-C. Ng, H.S.-O. Chan, Sens. Actuators, B 113 (2006) 234–240.
[20] L. Qin, X.-W. He, W.Y. Li, Y.-K. Zhang, J. Chromatogr., A 1187 (2008) 94–102.
[21] S. Thamizharasi, P. Gnanasundaram, K.V. Rao, A.V.R. Reddy, Eur. Poym. J. 32 (1996) 105–109.
[22] L.M. Cubillana-Aguilera, J.M. Palacios-Santander, I. Naranjo-Rodriquez, J.L. Hidalgo-Hidalgo-de-Cisneros, J. Sol–Gel Sci. Technol. 40 (2006) 55–64.
[23] D.A. Skoog, F.T. Holler, T.A. Neiman, Principles of Instrumental Analysis, 5th ed., Harcort Brace College Publishers, Orlando, 1998.
[24] M.A. Dikusar, I.V. Kubrakova, A.A. Chinarev, N.V. Bovin, Russ. J. Bioorg. Chem. 27 (2001) 408–412.
[25] X. Gao, Handbook on the Physics and Chemistry of Rare Earths 8 (1986) 163–201.
[26] X. Feás, J.A. Seijas, M.P. Vázquez-Tata, P. Regal, A. Cepeda, C. Fente, Anal. Chim. Acta 631 (2009) 237–244.
[27] D.S. Janiak, O.B. Ayyub, P. Kofinas, Macromolecules 42 (2009) 1703–1709.
[28] O. Ramström, L. Ye, P.-E. Gustavsson, Chromatographia 48 (1996) 197–202.
[29] K.B. Oldham, J. Electroanal. Chem. 122 (1981) 1–17.
[30] A. Babaei, M. Zendehdel, B. Khalizadeh, A. Taheri, Colloids Surf. B 66 (2008) 226–232.
[31] L. Meites, Polarographic Techniques, 2nd ed., Willey Intersciences, New York, 1965.
[32] A.J. Bard, L.R. Faulker, Electrochemical Methods, 2nd ed., Wiley, New York, 2001.
[33] W.M. Hassen, C. Martlet, F. Davis, S.P.J. Higson, A. Abdelghani, S. Helali, N.J. Renault, Sens. Actuators, B 124 (2007) 34–45.
[34] T. Alizadeh, M.R. ganjali, P. Norovi, M. Zare, A. Zeradtkar, Talanta 79 (2009) 1197–1203.
[35] A. Sengupta, R. mahalakshmi, N. Shamala, P. Balram, J. Peptide Res. 65 (2005) 113–119.
[36] S. Shahrokhian, L. Fotouchi, Sens. Actuators, B 123 (2007) 942–949.
[37] K.-J. Huang, C.-X. Xu, W.-Z. Xie, W. Wang, Colloids Surf., B 74 (2009) 167–171.